J Comput Aided Mol Des (2014) 28:735–749
DOI 10.1007/s10822-014-9755-x

Temperature effect on poly(dA).poly(dT): molecular dynamics simulation studies of polymeric and oligomeric constructs

Sanchita Mukherjee · Sangeeta Kundu · Dhananjay Bhattacharyya

Received: 18 February 2014 / Accepted: 19 May 2014 / Published online: 28 May 2014

Abstract Understanding unwinding and melting of double helical DNA is very important to characterize role of DNA in replication, transcription, translation etc. Sequence dependent melting thermodynamics is used extensively for detecting promoter regions but melting studies are generally done for short oligonucleotides. This study reports several molecular dynamics (MD) simulations of homopolymeric poly(dA).poly(dT) as regular oligonucleotide fragments as well as its corresponding polymeric constructs with water and charge-neutralizing counterions at different temperatures ranging from 300 to 400 K. We have eliminated the end-effect or terminal peeling propensity by employing MD simulation of DNA oligonucleotides in such a manner that gives rise to properties of polymeric DNA of infinite length. The dynamic properties such as basepairing and stacking geometry, groove width, backbone conformational parameters, bending, distribution of counter ions and number of hydrogen bonds of oligomeric and polymeric constructs of poly(dA).poly(dT) have been analyzed. The oligomer shows terminal fraying or peeling effect at temperatures above 340 K. The polymer shows partial melting at elevated temperatures although complete denaturations of basepairs do not take place. The analysis of cross strand hydrogen bonds shows that the number of N–H···O hydrogen bonds increases with increase in temperature while C–H···O hydrogen bond frequencies decrease with temperature. Restructuring of counterions in the minor groove with temperature appear as initiation of melting in duplex structures.

Keywords Hydrogen bonds · DNA melting · DNA oligomer · DNA polymer

Introduction

The formation of a double stranded (ds) DNA structure from two single DNA strands has been the subject of many biochemical and biophysical studies that have helped to elucidate the structure, thermodynamics and kinetics of dsDNA formation. The knowledge of DNA structure and its physicochemical properties is very crucial for understanding its role in living systems. DNA plays vital role in many biological processes such as replication, transcription, DNA repair etc. [1]. During these processes, dsDNA converts to single stranded form by unzipping mechanism. The biochemically active form of nucleic acid is the locally melted single stranded (ssDNA) conformation, where the greater conformational freedom of ssDNA compared to dsDNA drives the melting transition of DNA, that can promote localized strand separation or the formation of 'bubbles' [2]. The opening of the DNA double helix is therefore a prerequisite for replication and transcription of the genetic code. The relationship between DNA sequence, structure, and function has been studied and discussed extensively for the last two decades. Many high-resolution structures of dsDNA molecules have been determined mostly using X-ray crystallography, but the process of structure formation and characterization of intermediates of

Sanchita Mukherjee and Sangeeta Kundu have contributed equally to this work.

Electronic supplementary material The online version of this article (doi:10.1007/s10822-014-9755-x) contains supplementary material, which is available to authorized users.

S. Mukherjee · S. Kundu · D. Bhattacharyya (✉)
Computational Science Division, Saha Institute of Nuclear Physics, 1/AF Bidhannagar, Kolkata 700064, India
e-mail: dhananjay.bhattacharyya@saha.ac.in

dsDNA formation has not been structurally characterized due to the fact that structure formation processes may involve short-lived intermediate structures that are arduous or impossible to crystallize and to study experimentally at atomic resolution [1].

In the cellular environment there exist different proteins such as DNA or RNA polymerase, gyrase etc., which help the unzipping mechanism. However, DNA denaturates due to the larger entropy of the flexible single strands, which can most easily be achieved by increasing the temperature of the sample until the DNA melts. In living organisms, however, enzymes and other proteins may force the two strands apart, similar to thermally driven melting. In vitro experimental studies to understand these mechanisms often use melting induced by high temperature, for example, determination of promoters or origins of replication are often done using melting temperature data of several oligonucleotides [3–5]. Such systems could be studied by molecular dynamics (MD) simulations which has the capability of providing tremendous amount of useful information about the structural and dynamic properties of macromolecules [6, 7] as seen by recent state of art MD studies [8–13]. Thus simulations providing insights into thermal melting properties of several DNA duplexes have been done using coarse-grained models in the absence of ions and solvent [14, 15] as well as atomistic models with continuum solvent [1] and explicit water [16]. Reports dealing with MD simulation of oligomer at higher temperatures, such as, denaturation of Drew-Dickerson DNA dodecamer d(CGCGAATTCGCG) in a high salt concentration shows transition states of melting process involving the untwisting of DNA and peeling conformations [17]. MD simulation study of temperature-induced melting of duplex DNA in presence and absence of covalently bonded ligands showed that the drugs stabilises dsDNA [18]. Wong and Pettitt's [19] 100 ns simulation of DNA oligomer at 400 K provides an atomistic picture of how DNA oligomers melt in a realistic solution environment. However, most of the MD simulations of DNA are done for oligonucleotide fragments that mimic properties of those molecules studied by X-ray crystallography or NMR spectroscopy. The cellular and functional DNA molecules, however, exist mostly as polymers and their behaviour is analyzed only through few spectroscopic methods, gel electrophoresis, electron microscopy and other low resolution studies. MD simulation of DNA oligomers always show terminal fraying effect or peeling even at physiological temperature [19, 20] which leads to melting of DNA through a non-cooperative way as there is no need of high nucleation energy at the central basepairs for following of propagation of basepair opening on both sides of an unpaired region. Structures of a few DNA dodecamers with totally unpaired basepairs at both termini have also been solved by X-ray crystallography, as discussed earlier [21]. There were very few attempts to study nearly polymeric DNA by creating the water-box in such a manner that ends of the molecules in the periodic boundary condition (PBC) are stacked on top of one-another [22]. However these simulations also show peeling or fraying effect [21]. Absence of peeling conformations in the melting process of the polymeric DNA can show different melting signature as compared to its oligomeric counterpart. With this aim, we focused our attention to investigate the effect of temperature on DNA melting, both in case of oligomer as well as its corresponding polymer model. Our polymeric construct is expected to exhibit local melting at elevated temperatures.

In this current work we employed MD simulations for homopolymeric poly(dA).poly(dT) sequence which possesses several unique structural features. This sequence deserves special attention as it could not form nucleosomes in presence of histone octamers, possibly due to its structural rigidity as measured by its large persistence length [23, 24] and remains in linker regions between two nucleosomes [25]. Furthermore it could not induce the common B to A transition as this sequence does not adopt A-DNA conformation even in presence of dehydrating agent [26]. There are several proposed models of poly (dA).poly(dT) and these are not in agreement with each other [27–30]. The specific basepair orientations for this sequence may be responsible for intrinsic DNA curvature due to phased $dA_n.dT_n$ tracts [27, 31, 32], whereas the homopolymeric double helix is always straight. However, this issue is of particular biological significance as sequence dependent intrinsic DNA curvature is an important determinant of DNA recognition by proteins. Experimental studies demonstrated that unusual conformation of poly(dA).poly(dT) in solution exist at ambient temperatures and disappears when the temperature is increased [33, 34]. These [35] indicate a reversible transition from B′ conformation of poly(dA).poly(dT) to a new double helical structure (B*) at a relative humidity near 80 %, when the temperature is raised above 30 °C [33]. X-ray crystallographic structure of poly(dA).poly(dT) like stretch indicates possibility of cross strand bifurcated hydrogen bonds between successive basepairs which probably makes this structure rigid [23, 36]. Three centred cross strand hydrogen bond is formed by pairing of amino group (N6) of adenine with the carbonyl group (C4=O) of the Watson–Crick paired thymine and the carbonyl oxygen (C4=O) of thymine at the nearest neighbour [35, 36]. Pre-melting transition probably occurs due to breakage of the bifurcated cross strand hydrogen bond from adenine to the consecutive flanking thymine [35]. Thus we focused our attention to investigate the melting signature of this homopolymeric poly(dA).poly(dT) at different temperatures with an aim to

understand the difference between dynamic properties of the oligomer and the corresponding model polymer of infinite length using MD simulations.

Among several methods of constructing polymer in PBC we adopted one where the 3′ end of the DNA strand is connected to its periodic image along the z axis [37–39] as these constructs show regular variation in duplex parameters [21, 40]. Simulation of such endless DNA construction has been of recent interest in literature where DNA minicircles show melting behaviour [41]. In this model the duplex holds its B-DNA like structure which is the relaxed form and would prevent supercoiling under normal conditions as directed from its conserved linking number [42]. In the present study we performed 100 ns long MD simulations for the oligomer and 60 ns long MD simulations for the model polymer at several different temperatures between 300 and 400 K. The dynamic properties such as inter and intra basepair orientation parameters, groove width and backbone conformational parameters of the oligomeric and polymeric constructs have been determined along with ion distributions around the double helix. The force field effects are also evaluated by carrying out simulations using CHARMM-27 [43] and AMBER [44] parmbsc0 force-fields. We believe that our work provides a useful comparison between oligomeric and polymeric constructs of poly(dA).poly(dT) that may be helpful to understand the unzipping mechanism of DNA double helix.

Materials and methods

The initial structure of the 20-basepair-long B-DNA double helix of sequence $d(A_{20}).d(T_{20})$ was generated using fibre diffraction [45] derived structure. The chains were terminated at the 5′-end by –C5′–O5′–H and at the 3′-end by –C3′–O3′–H for oligomer simulations using conventional way. Another set of structures were terminated with –C5′–O5′–P(O1P)(O2P)– at the 5′-end and –C3′–O3′– at the 3′-end for simulations of polymer. We can abbreviate the two systems as AA-oligo and AA-poly respectively. The systems contained Na^+ ions in the exact number (38 for oligomers and 40 for polymeric constructs) required to achieve electro neutrality of the whole system. The positioning of the ions was determined by Monte Carlo (MC) simulation as described earlier [21, 40].

In most of the simulations, we used the empirical CHARMM-27 force field [43] to describe the biomolecular interactions, as it was shown that this force field maintains B-DNA like structures at ambient hydration [46]. MD simulations of the oligomers were performed using NAMD software [47, 48] while the corresponding polymers were simulated using CHARMM-35b6 software [49]. The simulation cell contains double helical 20 basepair long $d(A_{20}).d(T_{20})$ fragment with O3′ atom of the 3′-end of the DNA strand connected to its periodic image along the z axis by using "image patch (IMPAtch)" option of CHARMM, which forms covalent bond between O3′ and P mimicking a continuous DNA chain. For our system, we introduced two such pseudo covalent bonds: one between O3′ atom of the 20th adenine of the primary simulation box and P atom of the first adenine of the image box along the z direction. On the other strand we incorporated a bond between P atom of 21st thymine with the O3′ atom of the 40th thymine of the image box. The MD simulations of DNA along with charge-neutralizing counterions and water were carried out in an orthorhombic cell having dimension of $60 \times 60 \times 67.6$ Å^3 with PBC imposed in all directions. The dimension along the z axis (67.6 Å) ensures that the last basepair of the DNA in primary unit cell stacks well with the first basepair of its periodic image. The oligomeric simulations were also done with identical box size so that the last basepair has at least good stacking interaction with the first basepair of the periodic image. A 10 Å cut-off distance was applied to the non-bonded interactions. We have used particle mesh Ewald [50] method for treating the long range electrostatic interactions with a kappa value of 0.35. The system energy was first minimized by 100 steps of steepest descent, followed by 1,000 steps of conjugate gradient and 20,000 steps of adopted basis Newton–Raphson method. After energy minimization, each system was subjected to slow heating followed by production run of varying length within the temperature range of 300–400 K with 20° interval using the CPT ensemble (Table 1). The solvent bath of all the systems consisted of TIP3P [51] water molecules. Although it has been reported that more recent water models like TIP4P reproduces temperature effect better [52] than the other models, its behaviour as solvent of biomolecules is not tested rigorously. Hence we have used TIP3P, as several reports on high temperature simulations of proteins and nucleic acids solvated by TIP3P indicate its reasonable accuracy even at high temperatures [17–19, 53–56]. Temperature was controlled by the Hoover algorithm [57] with the mass of the thermal piston being 1,000.0 kcal ps^2, while the pressure was controlled by Langevin–Piston algorithm [58]. The MD simulations were carried out with a time step of 1 fs, without shake or any other constraints, as the motion of the hydrogen atoms is crucial for the important hydrogen bonds [59]. It is anticipated that at higher temperature the PBC boxes would expand in size but these expansions, particularly for the polymers can be along Z direction only stretching the DNA. We have therefore carried out MD simulations for 7 ns each for the polymeric constructs using CPT dynamics. These equilibrated volumes [21] of the systems at different temperatures are given in Table SI. These were then followed by MD simulations at constant volumes for 53 ns keeping the cell dimensions obtained by the 7 ns long CPT simulations at

Table 1 Total simulations done and corresponding root mean square deviation (RMSD)

System	Temperature (K)	Force field used	Simulation time (ns)	RMSD (Å)
AA-oligo	300	CHARMM 27	100	2.2 (0.4)
	320	CHARMM 27	100	2.2 (0.4)
	340	CHARMM 27	100	2.6 (0.5)
	360	CHARMM 27	100	5.1 (0.9)
	380	CHARMM 27	100	8.0 (0.5)
	400	CHARMM 27	100	16.3 (1.4)
AA-poly	300	CHARMM 27	60	1.9 (0.2)
	320	CHARMM 27	60	2.0 (0.2)
	340	CHARMM 27	60	1.9 (0.2)
	360	CHARMM 27	60	2.1 (0.3)
	380	CHARMM 27	60	2.0 (0.3)
	400	CHARMM 27	60	2.0 (0.3)
	300	Parmbsc0	60	1.8 (0.2)
	400	Parmbsc0	60	2.0 (0.4)

RMSDs are calculated for last 93 ns and last 53 ns for AA-oligo and AA-poly, respectively, for 300 K and last 10 ns for rest of the simulations at higher temperatures

the corresponding temperatures. Simulations of AA-poly were also carried out using AMBER parmbsc0 force field [44] at 300 and 400 K for 60 ns each. MD simulations for the AA-oligo were carried out for 100 ns each at six different temperatures using CPT dynamics. Altogether we have executed 1.08 μs simulation of the two systems under varying simulation conditions (Table 1). Trajectory analysis was performed using CHARMM. For 300 K, analyses were done for entire trajectory run after 7 ns CPT equilibrium simulations and for higher temperature simulations last 10 ns were considered. Snapshots taken in 1 ps intervals were analyzed using NUPARM software [60, 61]. From NUPARM outputs, time series of conformational parameters were extracted. These included six inter-basepair parameters (tilt, roll, twist, shift, slide and rise), six intra basepair parameters (open, buckle, propeller, shear, stagger and stretch) as well as groove widths (based on P–P distances), backbone torsions, and sugar puckers. The definitions and nomenclatures of these parameters can be obtained from the reports of IUPAC/IUB conventions [62–64]. Locations of counteractions and analysis of hydrogen bonds between bases were done by in-house developed FORTRAN programs.

Results and discussion

Previously we had performed 7 ns simulations of the oligomeric and polymeric poly(dA).poly(dT) and found that oligomer shows terminal fraying effects at higher temperatures even within 7 ns, but the polymers did not show melting feature [21]. It was also seen that expansion of volume of the periodic box with temperature followed expected trend, implying applicability of the force field at elevated temperatures. In the present study we extended the oligomeric runs to 100 ns and the polymeric runs to 60 ns. It is expected that at elevated temperatures, the structures would unfold, but a complete melting may take enormous time in terms of MD time scale (still, complete denaturation is observed for oligomeric simulation at 400 K). Thus the 60 or 100 ns simulations may provide transition profiles for most of the cases. We have therefore carried out structural analysis during last 10 ns for all the systems at the elevated temperatures. The structures corresponding to 300 K are, however, analyzed from equilibration time to ends of simulation.

Structure and stability at 300 K

We begin our study by looking at the overall stability of the oligomer and polymer conformations at 300 K. We examine the evolution of the structure during the simulation runs by calculating root mean square deviations (RMSD) of the trajectories with respect to the energy-minimized structures of the double helices. The RMSDs of the AA-oligo and AA-poly systems, with respect to the energy minimized structures indicate expected dynamics of the systems—the AA-oligo has somewhat higher mobility (Avg. RMSD = 2.2 Å) as compared to the AA-poly (Avg. RMSD = 1.9 Å). Elimination of the terminal basepairs in oligomer does not show much reduction in RMSD values indicating no peeling behaviour at 300 K. This indicates that, both the systems behave similarly at physiological temperature. The completely hydrated oligomeric systems, however, may behave differently from these [40].

The backbone torsion angles are calculated separately for the d(A) and d(T) strands as these may show significant asymmetry in values. There are variations in average values of α, β, γ and δ angles, where d(A) and d(T) strands differ systematically by 3°–10° in both polymer and oligomer. The nucleic acid backbone is considered to be in the BI form when $\varepsilon - \zeta$ is negative and in the BII form when it is positive. In BI form the corresponding ε and ζ angles are within 120°–210° (trans) and 235°–295° ($gauche^-$) respectively while for BII, ε becomes $gauche^-$ and ζ becomes trans. In this homopolymeric sequence all the residues are expected to adopt BI conformation at 300 K. We observe most of the sugars remain in C2′-endo puckered form. Distinct zones in phase angle (Table SII, SIII, SIV) are observed for adenine and thymine sugar residues; adenine sugar phase angles cluster at 155° and thymine sugar phases remain around 134° at 300 K for oligomer. Such clustering is also noticed in polymeric

construct where average pseudorotation phase angle values for adenine and thymine sugar residues are 159° (with standard deviation of 24°) and 138° (41) respectively. Experimental evidence also indicates sugar conformations in the refined Ca-poly(dA).poly(dT) structure are close to C2′-endo [27]. However, the sugars in both B* and αB′ conformation adopt C1′ exo puckering [33]. The glycosidic torsion χ however remains in preferred anti-conformation (χ around −120°). For polymer, average glycosidic torsion angle χ for d(T) is more negative than that of d(A) (average values are −112° (19) and −105° (13), respectively). This distinct difference between χ angles is also visible for oligomer at this temperature. Average value of χ for d(A) and d(T) chain are respectively −107° (14) and −115° (20) for oligomer at 300 K. We have analysed the conformational properties of the junction between the primary and image box created by P-O3′ pseudo-bonds using IMPAtch option of CHARMM. Regularity of the bond lengths and bond angles are observed as compared to rest of the structure. The torsion angles involving the P-O3′ bond also show similarity to the general variation with average α, ε and ζ torsions involving the pseudo bond having values of −62.5° (17.8), 220.3° (33.0) and 233.4° (42.9) respectively (Table SII) inferring the regularity of the end of the sequence in polymeric construct.

We have calculated all the intra- and inter-basepair parameters for both the polymer and the oligomer (Table SIV-SV). In case of intra basepair parameters the average buckle and propeller (Fig. 1) values for AA-oligo are −2.5° and −13.1° in the central region while these are −9.0° and −15.7° respectively in the terminals. Such variations, depending on positions of the basepairs, are much less for polymer in case of buckle and not at all present in case of propeller. These variations, however, do not indicate terminal melting or fraying of AA-oligo at 300 K which was intermittently seen in our earlier simulations [20]. Among the inter-basepair parameters roll values are found to be positive having average around 4° in both oligomer and polymer (Table SVa and Table SVIa). Average tilt (Fig. 2) values are non-zero (−2.3° for both AA-poly and AA-oligo) indicating absence of pseudo dyad symmetry between the two strands which is also clear in terms of torsion angles. Average twist values are slightly greater in polymer (35.5°) than oligomer (34.8°) and in oligomer the terminal basepair twist values are found higher by 1° than the central region. Twist values (Fig. 3), however, show less variation in case of AA-poly than AA-oligo where variation is found only at the terminals. For the 19th and the 20th (combining the 20th basepair and the linked image basepair) basepair step at the last terminal twist values are 32.6° (4.8) and 37.8° (5.0) respectively. This difference was unexpected as it was indicated even from solution experiments that poly(dA).poly(dT) have 10 basepairs per turn instead of 10.5 basepairs per turn for mixed sequence dsDNA [65]. Although we expected cylindrically symmetric structures of the polymeric sequence, the DNA undergoes significant deviations with random movement of the backbone and basepairs. This gives rise to dynamic curvature of the double helix. We have measured this curvature as angle between local helix axes of two terminal basepaired dinucleotides. The local helix axes between two basepairs were calculated by NUPARM [60]. These are defined by

$$\bar{Z}^{*} = \frac{(\bar{x}_1 - \bar{x}_2) \times (\bar{y}_1 - \bar{y}_2)}{|(\bar{x}_1 - \bar{x}_2) \times (\bar{y}_1 - \bar{y}_2)|}$$

where $\bar{y}_i$ (long axes) are obtained as the vectors connecting C8–C6 atoms of purines and pyrimidines of the basepair, $\bar{z}_i$ are basepair normals and $\bar{x}_i$ are obtained by $\bar{x}_i = \bar{y}_i \times \bar{z}_i$. Angles between first and last local helix axes are used to define bending angles of the oligonucleotides and this can give a good estimate of bending or curvatures in oligo or polynucleotides [66–68]. AA-oligo shows duplex bending angle of 17.01° (9.9). Even the uniformity in the AA-poly basepair parameters along the sequence is broken with the end-to-end bending of 15.75° (8.8) (Fig. 4a). This bending possibly gives rise to the small deviations of average twist from 36° (Fig. 3) and the small inequalities of the other parameters. This further indicates that the polymer construction did not make the DNA unrealistically rigid. However, the frequency distribution (histogram) of the end-to-end bending angles is found to be significantly different from normal or Gaussian distribution with χ^2 value of $6.739 \times 10^{+4}$ with 60 degrees of freedom (number of bins) (Figure SVII). This indicates that the bending is not intrinsic characteristic in this case; rather it may be generated from dynamic fluctuation.

B-DNA double helices are characterized by two deep grooves of unequal size and these are the sites for specific molecular recognition. In terms of groove width (Table 2), we noticed more uniformity of AA-poly as compared to AA-oligo. The average values are however similar in the two cases—AA-poly and AA-oligo both have narrow minor groove in terms of phosphate–phosphate distances of 12.8 Å (1.0) and 13.0 Å (1.9). Major groove of AA-oligo is found wider (17 Å ± 2.2) with a central narrowing which is not found in AA-poly (16.4 Å ± 1.4). There are no high-resolution structure of poly(dA).poly(dT), but its structure is expected to be similar to that of central AATT region of Dickerson dodecamer and its variants [36]. These structures were solved by single crystal X-ray diffraction and their minor groove widths at the central region are around 10 Å. We may therefore speculate that the structure of A-stretch DNA as modelled from knowledge of Dickerson dodecamer is probably different from that of longer A-stretch, such as poly(dA).poly(dT). The observed

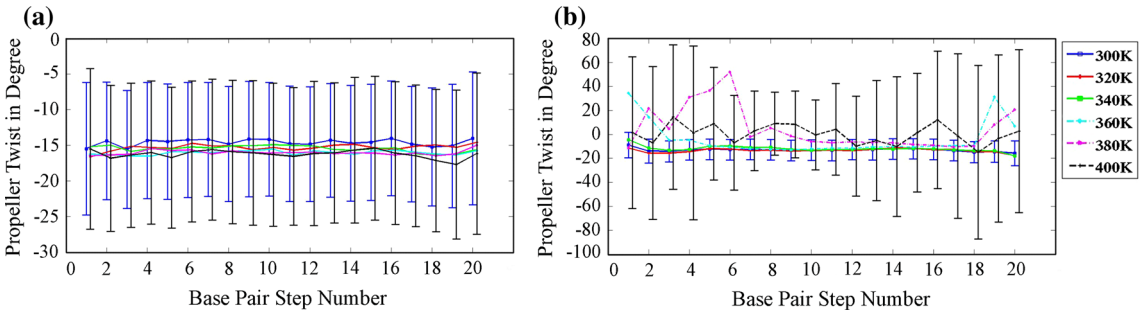

Fig. 1 Mean values of propeller twist for (**a**) AA-poly and (**b**) AA-oligo at different temperatures. The standard deviations for 300 and 400 K only are marked as *error-bars*. *Colour codes* for temperature are indicated beside the second panel (*b*)

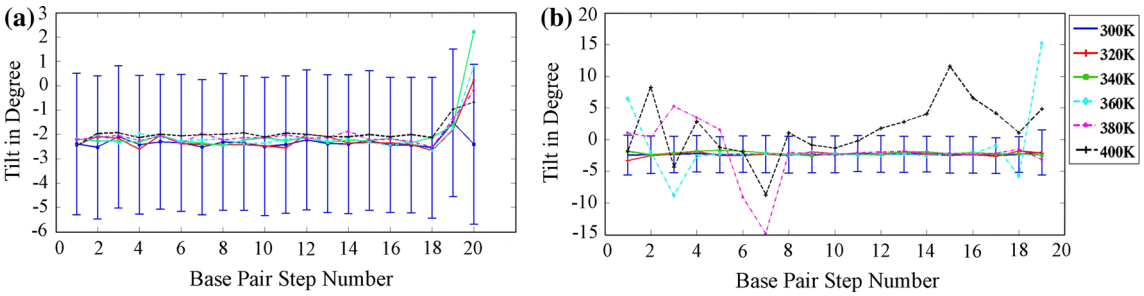

Fig. 2 Mean values of tilt for (**a**) AA-poly and (**b**) AA-oligo at different temperatures. The standard deviations for 300 K only are marked as *error-bars*. *Colour codes* for temperature are indicated beside the second panel (*b*). We have considered a virtual dinucleotide step consisting of 20:21 basepair of the primary DNA and the 1:40 basepair of the periodic image in case of AA-poly and calculated all the dinucleotide step parameters. The tilt value of the 20th step represents this step

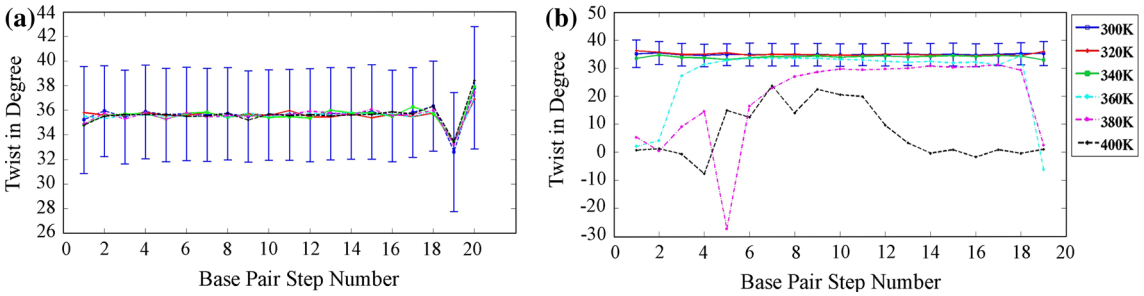

Fig. 3 Mean values of twist for (**a**) AA-poly and (**b**) AA-oligo at different temperatures. The standard deviations for 300 K only are marked as *error-bars*. *Colour codes* for temperature are indicated beside the second panel (*b*). We have considered a virtual dinucleotide step consisting of 20:21 basepair of the primary DNA and the 1:40 basepair of the periodic image in case of AA-poly and calculated all the dinucleotide step parameters. The twist value of the 20th step represents this step

structural features are, however, in agreement with other solution data [31, 69] as well as simulation data [70–72].

It was hypothesized that positively charged Na^+ ions may accumulate in the minor groove of A-tract DNA due to negative electrostatic potential of minor groove, which may reduce the minor groove width [73]. We have thus attempted to understand counterion dynamics around DNA. The average DNA structure comprising of entire simulation time is calculated. Each snapshot of DNA along with the Na^+ ions was reoriented by superposing the DNA duplex on this average structure and the corresponding ion positions were mapped with respect to the average structure of the duplex. Three dimensional small grids of dimension $(2\ \text{Å})^3$ were constructed to calculate the frequency of the Na^+ ions around DNA. After calculation of the grid frequency we have extracted 100 grids having highest grid frequencies and plotted the centre of the grids along with the average DNA structure (Fig. 5). In both the cases these high frequency grids are seen to be distributed along the minor groove (95 and 92 such points are near minor groove of AA-oligo and AA-poly, respectively). High frequency grids are very less in major groove and not at all present near phosphate residues. Maximum duration of ion occupancy was found to be 9.9 % of 53 ns total MD

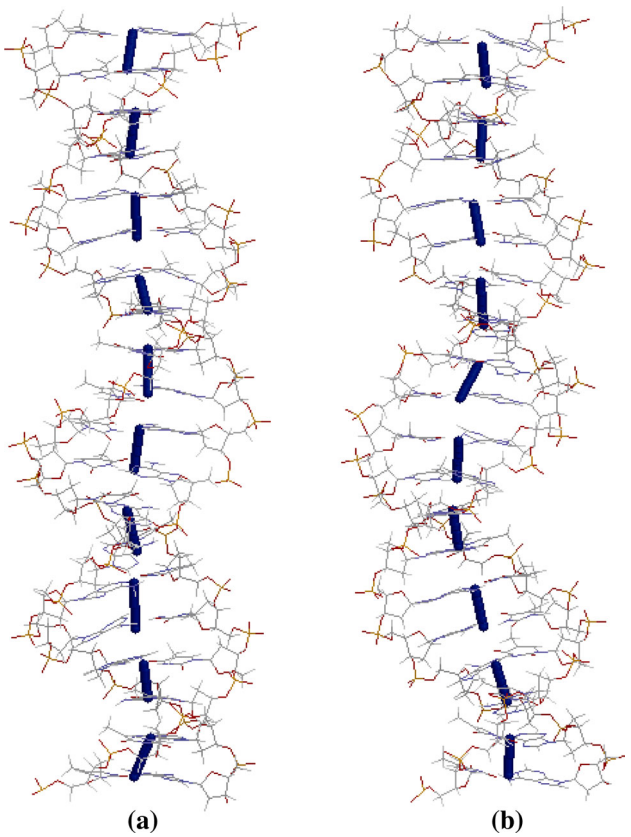

Fig. 4 Snapshots showing helical axis representative of bending in AA-poly with different end-to-end bending value: (**a**) at 300 K (15.9°) and (**b**) 400 K (20.2°)

near the polymer and 8.4 % of 93 ns total MD around the oligomer. This may indicate that movement of ions in polymer minor groove is more restricted than in the minor groove of the AA-oligo during the simulation run. This feature is correlated to slightly smaller minor groove of AA-poly.

The Watson–Crick (WC) and cross strand hydrogen bonds in the duplex structure (Table 3) are calculated with an in-house code. For WC hydrogen bonds angle greater than 150° and donor–acceptor distance cut-off of 3.5 Å have been adopted. The frequencies of N–H···O and N–H···N hydrogen bonds are comparably stable in polymer and oligomer simulations. Average number of the N–H···O and N–H···N hydrogen bonds for polymer are 16.24 (1.8) and 17.28 (1.6) respectively while these are 15.96 (1.9) and 17.13 (1.8) for AA-oligo. The frequency of N–H…N hydrogen bond is found higher than that of N–H···O as the former is more buried inside the duplex and hence suffer less fluctuation. Cross strand hydrogen bonds are also calculated with a relaxed criteria of angle >90° and H···A distance cut-off of 3 Å between successive basepairs as these imparts special consideration in the pre-melting mechanism of poly (dA).poly(dT) sequence [33, 35]. Among the three types of cross strand hydrogen bonds average number of N–H···O type hydrogen bonds is found more in polymer (4.8 ± 2.5) than in oligomer (3.2 ± 2.2). However, for polymer and oligomer, C–H···O and N–H···N hydrogen bonds show similar frequencies as the average number of these hydrogen bonds are 13.8 (2.1) and 5.0 (2.3) respectively for AA-poly and 13.0 (2.2) and 5.6 (2.3) respectively in AA-oligo. This observation is in agreement with previous analysis using crystal structure database studies [74].

Temperature effect on AA-oligo and AA-poly

RMSD analysis

RMSDs (Table 1) of AA-oligo increase considerably with increase in temperature and attain a value of 4.6 Å at around 2.6 ns at 360 K which becomes 7 Å at the end of the simulation (∼99 ns) indicating melting at this temperature. The AA-oligo at 360 K and higher temperatures exhibits tendency to give unstructured conformation in course of simulation as revealed by high RMSD values. The RMSDs of the oligomer increase from beginning of the MD simulation at 380 and 400 K. For AA-oligo at 400 K a sudden jump of RMSD is observed at around 88 ns from 17 to 34 Å due to strand separation of the DNA double helix at this time. On the contrary, RMSDs and their variances of AA-poly increase slightly at higher temperatures.

Table 2 Minor and major groove widths (in Å) of AA-poly and AA-oligo at different temperatures

System	Temp (K)	Minor groove	Major groove	System	Minor groove	Major groove
AA-poly				AA-oligo		
CHARMM	300	12.56 (1.1)	16.27 (1.4)		12.85 (2.1)	16.74 (2.3)
	320	12.89 (1.0)	16.12 (1.3)		12.98 (1.1)	17.12 (1.6)
	340	12.83 (1.1)	16.41 (1.4		13.23 (1.1)	17.55 (1.7)
	360	12.88 (1.1)	16.24 (1.4)		14.49 (2.0)	17.77 (2.3)
	380	12.87 (1.2)	16.50 (1.5)		18.43 (3.5)	18.91 (2.8)
	400	12.88 (1.3)	16.88 (1.6)		–	–
AMBER	300	10.06 (1.0)	19.15 (1.5)			
	400	11.16 (1.6)	18.73 (1.9)			

The groove widths are calculated as inter chain phosphate···phosphate distances across respective grooves

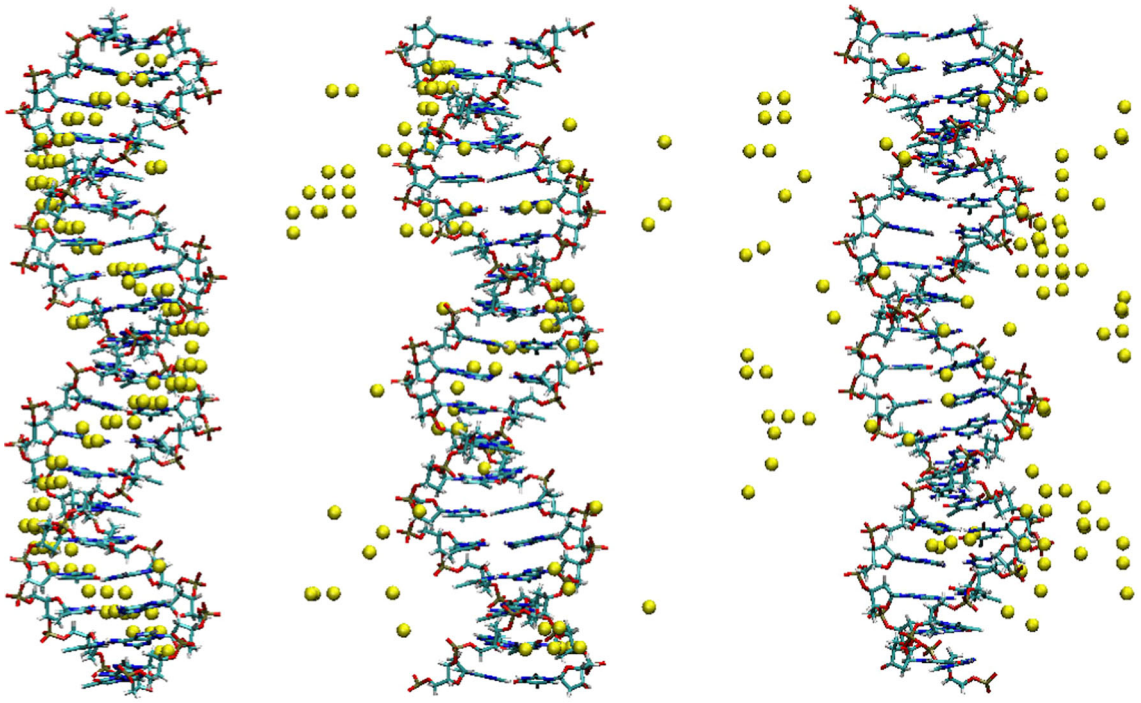

Fig. 5 Time-average structures of AA-poly along with Na^+ counterion locations as determined by 100 highest frequency grid centers at three different temperatures (**a**) 300 K, (**b**) 340 K and (**c**) 400 K

Table 3 Number of average Watson–Crick and cross strand hydrogen bonds with standard deviations in AA-poly and AA-oligo

Temp (K)	WC hydrogen bonds		Cross strand hydrogen bonds		
	N–H···O	N–H···N	N–H···O	C–H···O	N–H···N
AA-poly					
CHARMM					
300	16.24 (1.8)	17.28 (1.6)	4.77 (2.5)	13.80 (2.1)	4.99 (2.3)
320	15.85 (1.8)	17.17 (1.7)	5.36 (2.5)	13.96 (2.1)	5.32 (2.3)
340	15.23 (1.9)	17.04 (1.7)	5.62 (2.6)	13.22 (2.2)	4.94 (2.3)
360	14.88 (2.0)	16.93 (1.7)	6.44 (2.7)	13.30 (2.2)	5.11 (2.3)
380	14.31 (2.1)	16.78 (1.8)	6.38 (2.7)	12.45 (2.3)	4.83 (2.2)
400	13.70 (2.1)	16.67 (1.8)	6.69 (2.8)	11.49 (2.4)	4.49 (2.2)
AMBER					
300	17.38 (1.7)	18.61 (1.2)	3.65 (1.9)	16.59 (1.5)	3.03 (1.8)
400	15.99 (1.9)	17.19 (1.6)	4.43 (2.2)	13.34 (2.1)	3.02 (1.7)
AA-oligo					
CHARMM					
300	15.96 (1.9)	17.13 (1.8)	3.24 (2.2)	13.04 (2.2)	5.61 (2.3)
320	15.58 (1.9)	17.05 (1.7)	3.54 (2.1)	12.84 (2.2)	5.06 (2.3)
340	14.83 (2.0)	16.64 (1.8)	3.05 (2.1)	11.57 (2.4)	5.31 (2.3)
360	9.28 (3.5)	11.03 (3.6)	8.53 (5.8)	9.06 (2.5)	7.61 (3.9)
380	Slippage	Slippage	18.45 (3.5)	10.01 (3.8)	14.16 (2.4)

Backbone conformation

A detailed study of backbone conformation of the different systems gives a general idea about the conformational changes introduced in the sugar-phosphate backbone during the course of MD-run at different temperatures. Based on this a comparison could be made for AA-oligo and AA-poly at different temperatures. We observe most of the

d(A)-chain sugars remain in C2′-endo puckered form and d(T)-chain sugars in C1′-exo form. At higher temperatures, individual values of phase angle decrease for AA-oligo, but their conformations remain unchanged. Average value of pseudorotation phase angle for the sugars of the d(T) chain is found to be smaller than those of d(A) chain even at elevated temperature for AA-oligo. The difference between these two sugar-phosphate residues reduces with increase in temperature. As a result distinct clustering zones of phase angle for adenine and thymine sugar residues, observed at 300 K, gets diminished at higher temperature. Such clustering is also noticed in polymeric construct but the differences in phase angles between adenine-sugars and thymine-sugars remain unaltered with temperature for polymer. At 400 K, average values of sugar pucker phase angles for d(A) and d(T) chain for AA-poly are 155.3° (23) and 136.1° (21) respectively while for AA-oligo these two values become 136.6° (66) and 131.3° (47) respectively. Variations of phase angle values of individual bases are quite low both for d(A) and d(T) chain for AA-poly even at higher temperature. AA-oligo in contrast exhibits large variation of phase angles of individual residues. Fluctuations of phase values enhance with increase in temperature.

The glycosidic torsion (χ) for all the bases remains in preferred anti-conformation. Average glycosidic torsion angle for d(A) chain is smaller than that of d(T) chain for both AA-oligo and AA-poly, the pattern is reverse to that obtained for phase angle (Table SII-SIV). Difference between average χ angle of d(A) and d(T) chain are prominent for the polymer at all temperatures (Table SIV). This distinct difference between χ angles is visible for oligomer at lower temperatures (up to 360 K). At higher temperatures, this difference reduces. Our finding however is in agreement with the models of DNA based on low resolution X-ray fibre diffraction where the structures [33] give χ value near $-110°$ for B* and αB′ conformation of DNA. At 400 K the AA-oligo melts and the separated d(A) chain adopts syn glycosidic conformation ($\chi \sim -80°$). Average ε values for both oligomer and polymer remain at $\sim 188°$ up to 340 K. At higher temperature the value remains the same for polymer, but it gradually increases for AA-oligo and attains 189.0° (22.8), 196.8° (27.4) and 209.9° (41.5) respectively at 360, 380 and 400 K. At all temperatures, average ζ value for d(A) chain is smaller than d(T) chain both for AA-oligo and poly. Up to 340 K, average ζ value for AA-oligo remains at around 248° (22.8). A sudden drop of ζ value to 227° (46.5) is observed at 380 K for AA-oligo, which reduces further at 400 K and attains a value of 207° (59.3). Such drastic reduction of ζ value is not noticeable for AA-poly. Average value of ζ remains around 244° even at higher temperatures for AA-poly. Thus the AA-poly chiefly exists in BI conformation at all temperatures. The AA-oligo also exist in BI conformation, however at higher temperature (380 K) few BII like conformations are also available. The α/γ crankshaft motion maintains the canonical g−/g+ conformation at all temperatures for AA-poly. For AA-oligo, few residues adopt non-canonical g+/g+ conformation at elevated temperatures (at 400 K).

Basepair parameters

Time evolution of all the intra- and inter-basepair parameters for both the polymer and the oligomer has been determined at all temperatures. Interestingly the basepair parameters are more stable over the time period for polymer. The basepair parameter values of the terminal bases are quite different as compared to those of the central bases for AA-oligo. This effect is more pronounced at higher temperature (380 K onwards). In general the standard deviations of all intra and inter-basepair parameters increase with temperature for AA-oligo (Figs. 1, 2, 3). Average values of a few parameters such as propeller, local twist, rise, slide, and roll show a systematic variation with temperature for the oligomer simulations. Figure 1 shows the mean values of propeller twist for each of the basepairs of AA-poly and stacked AA-oligo at different temperatures with their standard deviations as error-bars. Average values of propeller remain around $-15°$ up to 340 K for the polymeric construct. While it becomes more negative ($-16°$) at elevated temperatures (360–400 K) (Fig. 1a). The effect of temperature is better reflected in the fluctuations of propeller twist in case of AA-poly. It takes anomalous values at higher temperatures for oligomers (Fig. 1b). It is clearly evident that average propeller twist values of all the basepairs are lower in polymer than the corresponding oligomer. It is also evident that six 5′-terminal and three 3′-terminal residues of AA-oligo do not remain in paired form at 380 K. The model of B* DNA for poly(dA).poly(dT) at elevated temperature has $-17°$ propeller [33], close to our MD value. It may be noted that B′-DNA for poly(dA).poly(dT) at lower temperature is supposed to have even larger negative propeller ($-22°$) [29], which allows them to form cross strand bifurcated hydrogen bonds between successive basepairs [23, 36].

Figure 6 shows time evolution of open angle of the five terminal basepairs of AA-oligo at 380 K as representative. This indicates terminal fraying of the oligomer at higher temperatures. This further shows that the unusually large value of open of the terminal basepair induces large value to the neighbouring one, which also induces large open to the next neighbouring one and so on. It becomes evident from Fig. 6 that unfolding propagates both from 5′-terminal as well as 3′-terminal ends. We observe that 1st, 2nd and 3rd basepairs of the oligomer undergo melting at 35, 45 and 95 ns respectively at 360 K (Figure SVIII). This melting process is accelerated at 380 K and the three

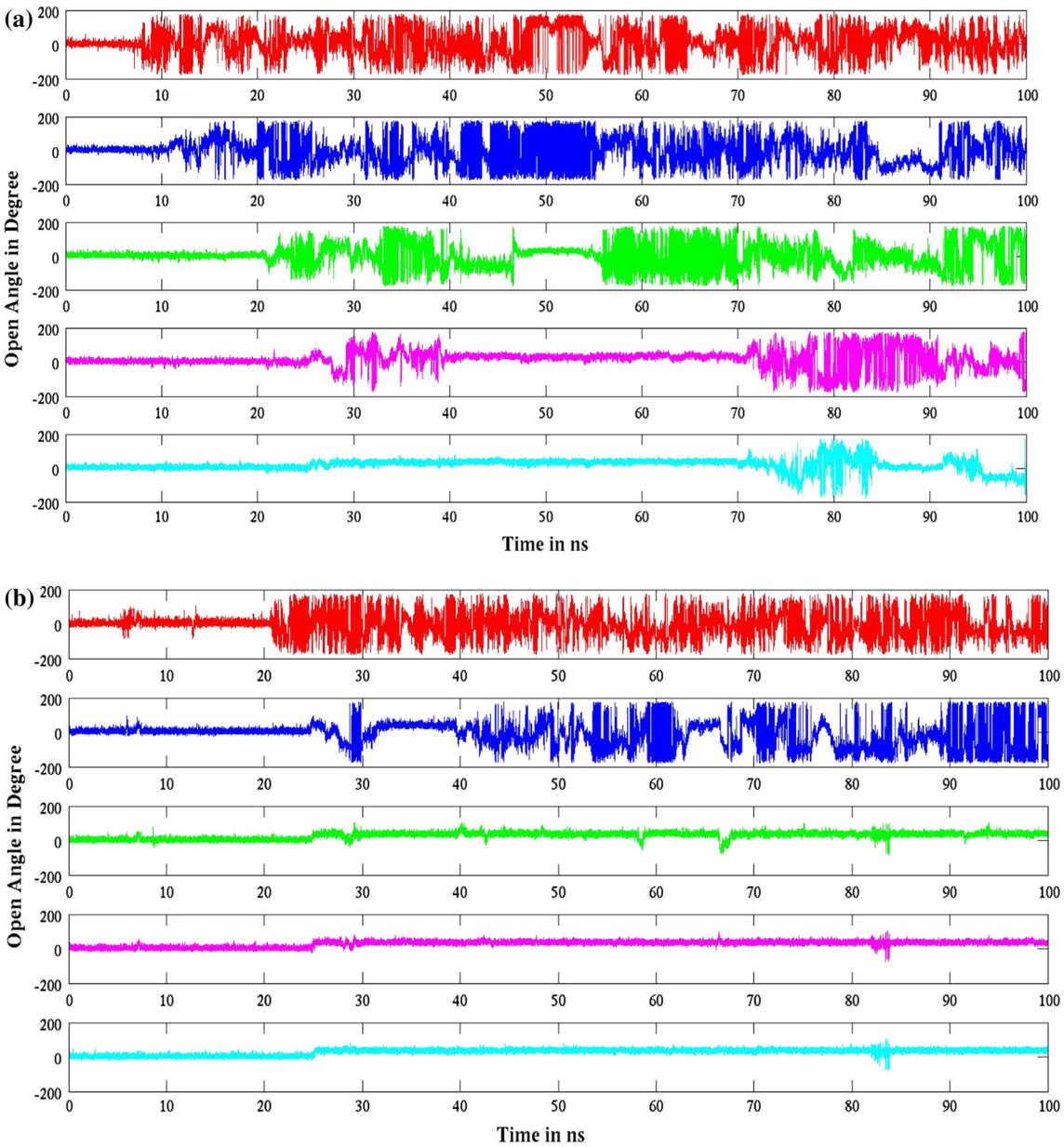

Fig. 6 Time evolution of open angle of the five terminal base pairs for AA-oligo at 380 K showing melting from both the termini. (**a**) Basepairs at 5′-end, (**b**) 3′-end

terminal basepairs melt at 10, 15 and 25 ns respectively at 380 K. During the next few nanoseconds, Watson–Crick pairs of the central region stochastically break and re-anneal, propagating the unpaired base toward the opposite end of the DNA, and slipping the entire DNA strand with respect to the other by 1 bp. Despite the slippage, the central bases remain stable and paired. This slippage is also observed at 400 K at around 27 ns. The twenty-mer AA-oligo becomes unstructured within 85 ns at 380 K, although ten basepairs of it remain stable up to 100 ns. At 400 K (Figure SIX), three terminal basepairs exist for 8, 10 and 12 ns. Thus the melting process speeds up with enhancement of temperature.

In order to determine when a basepair melts, we have calculated average and standard deviation of each of the basepair parameters for 1 ns interval. The melting point of the basepair is considered as the particular 1 ns duration when standard deviation of any basepair parameter value becomes five times the standard deviation of the same parameter at 300 K. The durability of each of the basepair steps has been plotted at different temperatures (Fig. 7). It shows basepair durability at different temperatures for AA-

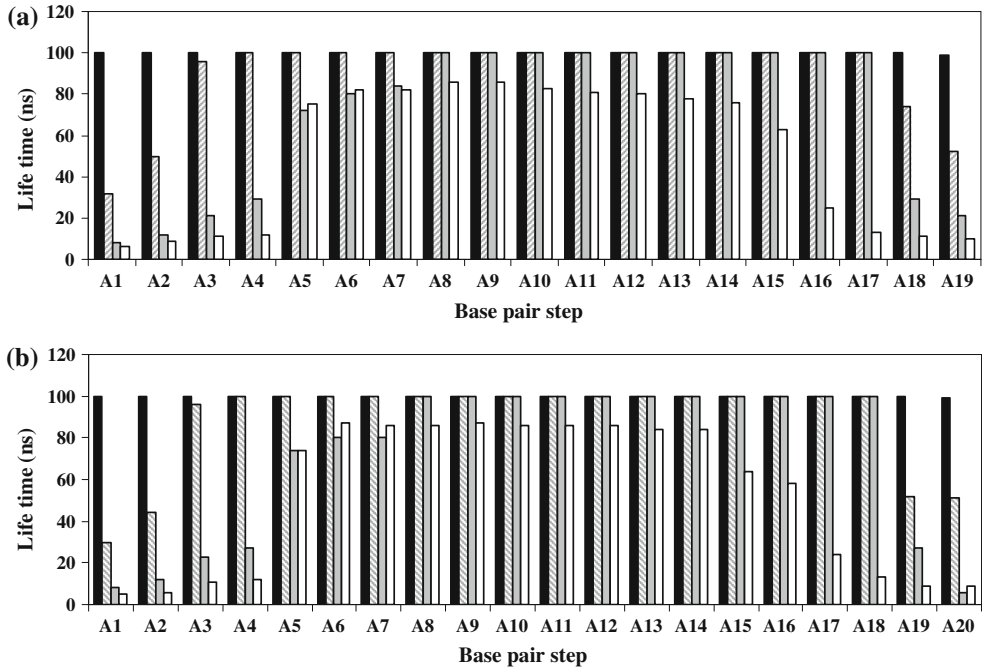

Fig. 7 Life time of individual base pairs of AA-oligo for (**a**) roll and (**b**) open angle at 340 K (*black*), 360 K (*lined*), 380 K (*grey*) and 400 K (*white*)

oligo for roll and open angle values, both indicating similar feature. At 360 K, melting involves only two pairs of terminal basepairs within 100 ns. Higher temperature onwards denaturation involves terminal as well as central basepairs. As expected life times of individual basepairs reduce at higher temperatures. Similar illustrations are also obtained for other basepair parameter values (data not shown).

At elevated temperature (360 K onwards) roll values of terminal basepairs become negative, while that of central basepairs remain positive for AA-oligo. For the polymeric construct average roll, tilt and twist (Fig. 3) values remain at around 4°, −2° and 35° respectively at all temperatures. Average tilt values are non-zero (around −2°) for AA-oligo up to 340 K, while at higher temperatures average tilt values become large positive for the terminal basepairs. Average twist angle for the oligomer is 34° (4.3) at 340 K. Average twist reduces systematically with hike in temperature for the oligomer (Fig. 3b). Such untwisting of DNA oligonucleotides at 400 K was also reported earlier [19]. Melting or pre-melting of AA-poly possibly requires even larger simulation time, but this could not be achieved as CHARMM requires considerably more computational time at the moment as compared to NAMD.

Hydrogen bond analysis with temperature

Hydrogen bonds are one of the key stabilizing forces in DNA double helical structure. Thus we have analyzed disruption of WC Hydrogen bonds in all the simulations (Table 3). We found that number of WC Hydrogen bonds reduces with temperature for both AA-oligo and AA-poly, as expected. We observed that for AA-oligo average number of N–H···O hydrogen bonds reduce from 15.96 at 300 K to 9.28 at 360 K. Similar trend is also seen in AA-poly where decrease of number of hydrogen bonds with temperature is less (16.26 at 300 K to 13.70 at 400 K). The N–H···N hydrogen bonds, however, do not reduce significantly in either systems (17.39 at 300 K and 16.67 at 400 K in AA-poly). This indicates that the AA-poly also undergoes partial melting but these do not affect the basepair parameters significantly. This feature is also reflected in the values of standard deviations of open angles, which systematically increase with temperature (Table SVI).

The analysis of cross strand hydrogen bonds shows that the number of N–H···O hydrogen bonds increases with increase in temperature (Table 3) while C–H···O hydrogen bonds decrease with temperature and N–H···N cross strand hydrogen bonds remains almost unaffected in case of AA-poly. This observation can be correlated with increase in propeller twist in the MD trajectories with temperature. In simulation of AA-oligo however the cross strand hydrogen bond frequencies do not change much up to 340 K (except C–H···O) and after 360 K it increases rapidly. Such increase in cross strand hydrogen bonds may arise due to enhanced fluctuation of the duplex with increasing temperature.

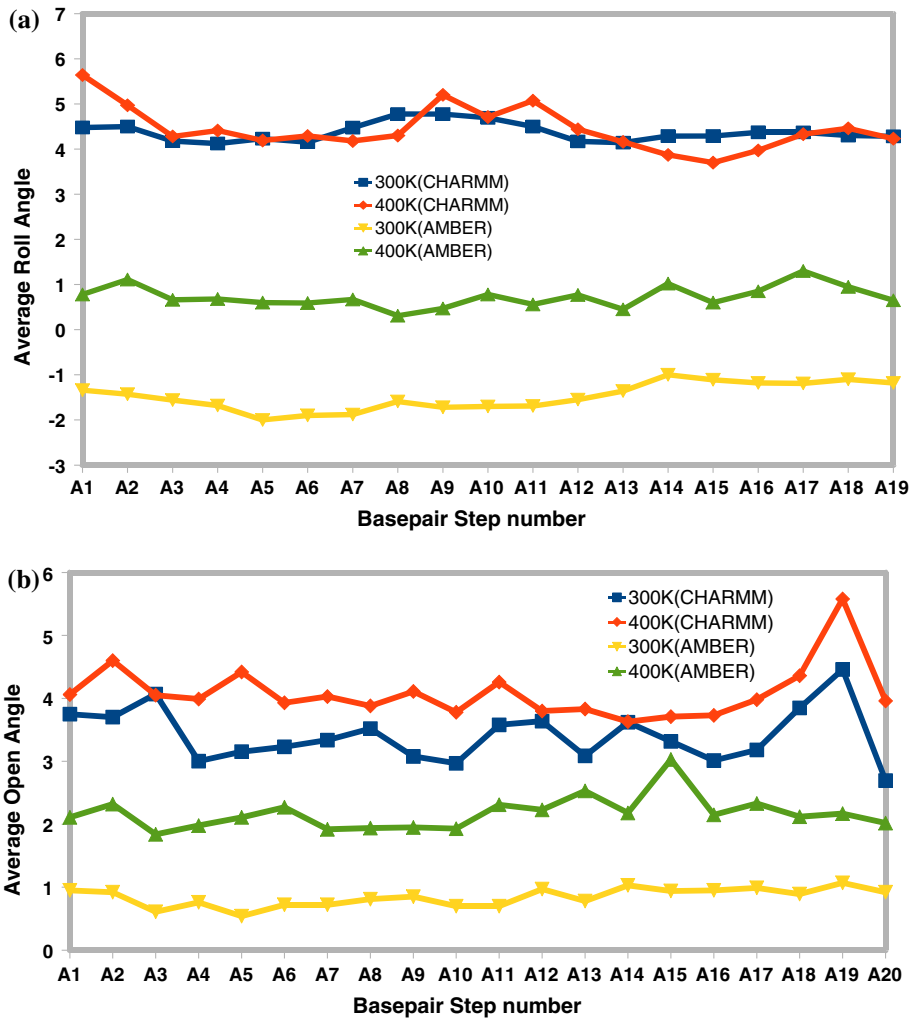

Fig. 8 Average values of (**a**) roll and (**b**) open angle for each of the 20 basepairs of AA-poly at 300 and 400 K with CHARMM and AMBER force-fields

The variation in base sequence is mostly manifested by alternation of stacking geometry and also formation of cross strand bifurcated hydrogen bonds between successive basepairs. However the disruption of the cross strand hydrogen bonds leading to pre-melting [33] was not observed in our simulations and hence we wanted to verify the simulations by using a different force field. We have carried out MD simulations of AA-poly at 300 and 400 K for 60 ns each using AMBER parmbsc0 force field. In almost all the cases results from AMBER simulations are similar to those from CHARMM parameters. Distribution pattern of χ and phase angles of d(A) and d(T) chains are similar to those obtained by CHARMM force field. BI conformation prevails in all simulations. However, roll and open angle values differ in CHARMM and AMBER simulations (Fig. 8). Propeller twist value becomes more negative in AMBER simulations ($-16.6°$ at 300 K and $-18°$ at 400 K). Minor groove width is narrower for AMBER simulation—average value of minor and major groove widths at 300 and 400 K are respectively 10.0 (1.0) and 11.1 (1.6) Å; and 19.1 (1.5) and 18.7 (1.9) Å. Nevertheless we get the similar variation of cross strand hydrogen bonds in AA-poly at 300 and 400 K with AMBER (Table 3) as propeller twist becomes more negative with temperature for both the force-fields.

Groove widths, bending and distribution of counterions with temperature

We found that the minor and major groove widths for the polymer vary little with increase in temperature (Table 2). The average values of minor and major groove widths for AA-poly are $\sim$12.8 and $\sim$16 Å, respectively, at all elevated temperatures and their fluctuations show steady increase with temperature. However, AMBER simulations show narrower minor groove widths. Similar effect is also seen for AA-oligo, but the effect appeared to be enlarged due to terminal fraying.

The end-to-end bending angles (as discussed in "Structure and stability at 300 K" section) for AA-poly at different temperatures are given in Table 4. This shows that the variations of curvature are comparable for polymer

Table 4 Average values of end-to-end bending angles (in °) for the systems at different temperatures

	AA-poly						AA-oligo
	300 K	320 K	340 K	360 K	380 K	400 K	300 K
End-to-end (20 bp)	15.75 (8.8)	14.54 (8.11)	16.39 (9.13)	15.63 (8.6)	17.27 (9.4)	20.21 (11.8)	17.01 (9.9)
Without terminal (16 bp)	14.02 (7.8)	14.01 (7.8)	14.69 (8.2)	15.10 (8.5)	16.05 (9.0)	17.05 (9.6)	15.23 (8.4)

and oligomer at 300 K as this calculation provides the dynamic curvature and is often unable to provide particular preferred bend. For oligomer, due to terminal fraying such end-to-end bending angle calculation becomes impossible beyond 300 K. Even though the terminals are constrained in the AA-poly system, the dynamic curvature increases with temperature (Fig. 4).

Distribution of ions around space was calculated in the same fashion as for 300 K. Unlike the simulations with 300 K for all other temperatures last 10 ns of simulation snapshots were taken into account to calculate the ionic distribution. At 320 K the spine of ion grids along minor grooves of AA-poly is found to be similar to that at 300 K. Although most of the high frequency grids remain in minor groove (72 %), some are also found in major groove (14 %) as well as near phosphate residues (10 %). At 340 K (Fig. 5) the 100 highest grid frequency points are scattered and no specific clustering in the minor groove (only 20 %) is seen and the mean grid frequency also reduces (0.43 %). Above this temperature no specific pattern is seen in case of AA-poly sequence. This also indicates a tendency of the AA-poly to melt above 340 K but the nucleation of melting did not take place. For AA-oligo at 320 K also spine of ion grids along minor grove is little disrupted compared to that of 300 K and high frequency points appear in major groove (17 %) as well as near phosphate residue (2 %). This feature remains unaltered in 340 and 360 K. At 380 K the spine of high frequency ion grids along minor groove completely disrupts.

Conclusion

This study establishes the usefulness of polymeric simulation [40] in terms of the stability imparted by restriction of terminal fraying. Computer simulation of polymeric molecule of nearly infinite length is always difficult and we adopted one of the possible methods to address it. As for example, it would be difficult to simulate A-form nucleic acid double helical structures by this method. We have tried to confine terminal opening in oligomers by placing the terminals of the duplex with the nearest basepair of the image at stacked position without real bonds. However in all the oligomer simulations the duplex show opening only at the terminals. Simulations with CHARMM, as well as AMBER force-fields do not display local denaturation and bubble formation at higher temperature in polymer simulations within 60 ns timescale. However, the hydrogen bond, bending and ion distribution analyses of the simulations indicate that the AA-poly also undergoes partial melting although basepair parameters do not show significant variation. The basepair disruption governing bubble formation is probably not observed as performing the simulations under conditions similar to those used in the real-life experiments until complete separation of the two strands and attaining convergence is currently unfeasible given the time scale of melting process, as also observed in recent MD studies [18]. It should be noted here that temperature and denaturant induced protein unfolding studies, as reported by several groups, also indicate need of longer time or more adverse conditions like higher temperature [75]. However, such adverse conditions may force the biomolecules to adopt alternate pathways for unfolding. We have therefore restricted our study to realistic temperatures.

We did not observe significant cross strand hydrogen bond in the simulation at 300 K, which was speculated to be an important component for DNA structural rigidity. Similar observation was also reported earlier [70–72]. It was shown by various studies that pyramidalization of amino groups may increase strength and hence stability of such cross strand hydrogen bonds [76–78]. The molecular mechanics force-fields, however, do not consider such pyramidalization, which possibly give rise to rather smaller propeller twists at physiological condition. Moreover, the fibre models of B′ and B*-DNA are obtained for DNA at 80 % relative humidity, where electrostatic interactions (a major component in hydrogen bonding) is expected to be stronger. We expect that consideration of amino group pyramidalization in the MM force-fields may improve the agreement between experimental and simulation results.

We observed major restructuring of counterions in the minor groove with temperature. This alteration [79] of spine of counterions also may be an important factor for increased flexibility or pre-melting of poly(dA).poly(dT) with temperature. It would be interesting to address this question from other theoretical as well as experimental studies.

References

1. Kannan S, Zacharias M (2009) Simulation of DNA double-strand dissociation and formation during replica-exchange molecular dynamics simulations. Phys Chem Chem Phys 11(45):10589–10595
2. Zeng Y, Zocchi G (2006) Mismatches and bubbles in DNA. Biophys J 90(12):4522–4529
3. SantaLucia J Jr (1998) A unified view of polymer, dumbbell, and oligonucleotide DNA nearest-neighbor thermodynamics. Proc Natl Acad Sci USA 95(4):1460–1465
4. Khandelwal G, Jayaram B (2010) A phenomenological model for predicting melting temperatures of DNA sequences. PLoS One 5(8):12433. doi:10.1371/journal.pone.0012433
5. Rangannan V, Bansal M (2011) PromBase: a web resource for various genomic features and predicted promoters in prokaryotic genomes. BMC Res Notes 4:257
6. Seibel GL, Singh UC, Kollman PA (1985) A molecular-dynamics simulation of double-helical B-DNA including counterions and water. Proc Natl Acad Sci USA 82(19):6537–6540
7. Leach A (2001) Molecular modelling: principles and applications. Pearson Education Limited, Dorchester, UK
8. Perez A, Luque FJ, Orozco M (2007) Dynamics of B-DNA on the microsecond time scale. J Am Chem Soc 129(47):14739–14745
9. Beveridge DL, Barreiro G, Byun KS, Case DA, Cheatham TE, Dixit SB, Giudice E, Lankas F, Lavery R, Maddocks JH, Osman R, Seibert E, Sklenar H, Stoll G, Thayer KM, Varnai P, Young MA (2004) Molecular dynamics simulations of the 136 unique tetranucleotide sequences of DNA oligonucleotides. I. Research design and results on d(C(p)G) steps. Biophys J 87(6):3799–3813
10. Dixit SB, Beveridge DL, Case DA, Cheatham TE, Giudice E, Lankas F, Lavery R, Maddocks JH, Osman R, Sklenar H, Thayer KM, Varnai P (2005) Molecular dynamics simulations of the 136 unique tetranucleotide sequences of DNA oligonucleotides. II: sequence context effects on the dynamical structures of the 10 unique dinucleotide steps. Biophys J 89(6):3721–3740
11. Arauzo-Bravo MJ, Fujii S, Kono H, Ahmad S, Sarai A (2005) Sequence-dependent conformational energy of DNA derived from molecular dynamics simulations: toward understanding the indirect readout mechanism in protein-DNA recognition. J Am Chem Soc 127(46):16074–16089
12. Fujii S, Kono H, Takenaka S, Go N, Sarai A (2007) Sequence-dependent DNA deformability studied using molecular dynamics simulations. Nucleic Acids Res 35(18):6063–6074
13. Drsata T, Perez A, Orozco M, Morozov AV, Sponer J, Lankas F (2013) Structure, stiffness and substates of the Dickerson–Drew dodecamer. J Chem Theory Comput 9(1):707–721
14. Drukker K, Schatz GC (2000) A model for simulating dynamics of DNA denaturation. J Phys Chem B 104(26):6108–6111
15. Linak MC, Dorfman KD (2010) Analysis of a DNA simulation model through hairpin melting experiments. J Chem Phys 133(12):125101. doi:10.1063/1.3480685
16. Perez A, Orozco M (2010) Real-time atomistic description of DNA unfolding. Angew Chem Int Ed Engl 49(28):4805–4808
17. Izanloo C, Parsafar GA, Abroshan H, Akbarzadeh H (2011) Denaturation of Drew–Dickerson DNA in a high salt concentration medium: molecular dynamics simulations. J Comput Chem 32(16):3354–3361
18. Bueren-Calabuig JA, Giraudon C, Galmarini CM, Egly JM, Gago F (2011) Temperature-induced melting of double-stranded DNA in the absence and presence of covalently bonded antitumour drugs: insight from molecular dynamics simulations. Nucleic Acids Res 39(18):8248–8257
19. Wong KY, Pettitt BM (2008) The pathway of oligomeric DNA melting investigated by molecular dynamics simulations. Biophys J 95(12):5618–5626
20. Mukherjee S, Bhattacharyya D (2013) Influence of divalent magnesium ion on DNA: molecular dynamics simulation studies. J Biomol Struct Dyn 31(8):896–912
21. Kundu S, Mukherjee S, Bhattacharyya D (2012) Effect of temperature on DNA double helix: an insight from molecular dynamics simulation. J Biosci 37(3):445–455
22. Bevan DR, Li LP, Pedersen LG, Darden TA (2000) Molecular dynamics simulations of the d(CCAACGTTGG)(2) decamer: influence of the crystal environment. Biophys J 78(2):668–682
23. Bhattacharyya D, Kundu S, Thakur AR, Majumdar R (1999) Sequence directed flexibility of DNA and the role of cross-strand hydrogen bonds. J Biomol Struct Dyn 17(2):289–300
24. Kunkel GR, Martinson HG (1981) Nucleosomes will not form on double-stranded RNA or over poly(dA).poly(dT) tracts in recombinant DNA. Nucleic Acids Res 9(24):6869–6888
25. Rhodes D (1979) Nucleosome cores reconstituted from poly(dA-dT) and the octamer of histones. Nucleic Acids Res 6(5):1805–1816
26. Pilet J, Blicharski J, Brahms J (1975) Conformations and structural transitions in polydeoxynucleotides. Biochemistry 14(9):1869–1876
27. Alexeev DG, Lipanov AA, Skuratovskii IY (1987) Poly(dA).poly(dT) is a B-type double helix with a distinctively narrow minor groove. Nature 325(6107):821–823
28. Arnott S, Selsing E (1974) Structures for polynucleotide complexes poly(dA). poly(dT) and poly(dT).poly(dA).poly(dT). J Mol Biol 88(2):509–521
29. Park HS, Arnott S, Chandrasekaran R, Millane RP, Campagnari F (1987) Structure of the alpha-form of poly[d(A)].poly[d(T)] and related polynucleotide duplexes. J Mol Biol 197(3):513–523
30. Arnott S, Chandrasekaran R, Hall IH, Puigjaner LC (1983) Heteronomous DNA. Nucleic Acids Res 11(12):4141–4155
31. Bolshoy A, McNamara P, Harrington RE, Trifonov EN (1991) Curved DNA without A–A: experimental estimation of all 16 DNA wedge angles. Proc Natl Acad Sci USA 88(6):2312–2316
32. Crothers DM, Haran TE, Nadeau JG (1990) Intrinsically bent DNA. J Biol Chem 265(13):7093–7096
33. Premilat S, Albiser G (1997) X-ray fibre diffraction study of an elevated temperature structure of poly(dA).poly(dT). J Mol Biol 274(1):64–71
34. Puhl HL, Behe MJ (1995) Poly(dA)·poly(dT) forms very stable nucleosomes at higher temperatures. J Mol Biol 245(5):559–567
35. Chan SS, Austin RH, Mukerji I, Spiro TG (1997) Temperature-dependent ultraviolet resonance Raman spectroscopy of the pre-melting state of dA.dT DNA. Biophys J 72(4):1512–1520
36. Nelson HCM, Finch JT, Luisi BF, Klug A (1987) The structure of an oligo(dA).oligo(dT) tract and its biological implications. Nature 330(6145):221–226
37. Korolev N, Lyubartsev AP, Laaksonen A, Nordenskiold L (2003) A molecular dynamics simulation study of oriented DNA with polyamine and sodium counterions: diffusion and averaged binding of water and cations. Nucleic Acids Res 31(20):5971–5981
38. Cheng Y, Korolev N, Nordenskiold L (2006) Similarities and differences in interaction of K^+ and Na^+ with condensed ordered DNA. A molecular dynamics computer simulation study. Nucleic Acids Res 34(2):686–696
39. Dai L, Mu Y, Nordenskiold L, van der Maarel JR (2008) Molecular dynamics simulation of multivalent-ion mediated attraction between DNA molecules. Phys Rev Lett 100(11):118301
40. Samanta S, Mukherjee S, Chakrabarti J, Bhattacharyya D (2009) Structural properties of polymeric DNA from molecular dynamics simulations. J Chem Phys 130(11):115103. doi:10.1063/1.3078797
41. Mitchell JS, Laughton CA, Harris SA (2011) Atomistic simulations reveal bubbles, kinks and wrinkles in supercoiled DNA. Nucleic Acids Res 39(9):3928–3938

42. Saenger W (1984) Principles of nucleic acid structure. Springer, New York
43. Foloppe N, MacKerell AD (2000) All-atom empirical force field for nucleic acids: I. Parameter optimization based on small molecule and condensed phase macromolecular target data. J Comput Chem 21(2):86–104
44. Perez A, Marchan I, Svozil D, Sponer J, Cheatham TE, Laughton CA, Orozco M (2007) Refinement of the AMBER force field for nucleic acids: improving the description of alpha/gamma conformers. Biophys J 92(11):3817–3829
45. Chandrasekaran R, Arnott S (1996) The structure of B-DNA in oriented fibers. J Biomol Struct Dyn 13(6):1015–1027
46. MacKerell AD, Banavali NK (2000) All-atom empirical force field for nucleic acids: II. Application to molecular dynamics simulations of DNA and RNA in solution. J Comput Chem 21(2):105–120
47. Kale L, Skeel R, Bhandarkar M, Brunner R, Gursoy A, Krawetz N, Phillips J, Shinozaki A, Varadarajan K, Schulten K (1999) NAMD2: greater scalability for parallel molecular dynamics. J Comput Phys 151(1):283–312
48. Nelson M, Humphrey W, Kufrin R, Gursoy A, Dalke A, Kale L, Skeel R, Schulten K (1995) MDScope—a visual computing environment for structural biology. Comput Phys Commun 91(1–3):111–133
49. Brooks BR, Bruccoleri RE, Olafson BD, States DJ, Swaminathan S, Karplus M (1983) CHARMM—a program for macromolecular energy, minimization, and dynamics calculations. J Comput Chem 4(2):187–217
50. Darden T, York D, Pedersen L (1993) Particle mesh Ewald—an N.Log(N) method for Ewald sums in large systems. J Chem Phys 98(12):10089–10092
51. Jorgensen WL, Chandrasekhar J, Madura JD, Impey RW, Klein ML (1983) Comparison of simple potential functions for simulating liquid water. J Chem Phys 79(2):926–935
52. Jorgensen WL, Jenson C (1998) Temperature dependence of TIP3P, SPC, and TIP4P water from NPT Monte Carlo simulations: seeking temperatures of maximum density. J Comput Chem 19(10):1179–1186
53. Izanloo C, Parsafar GA, Abroshan H, Akbarzade H (2011) Calculation of melting temperature and transition curve for Dickerson DNA dodecamer on the basis of configurational entropy, hydrogen bonding energy, and heat capacity: a molecular dynamics simulation study. J Iran Chem Soc 8(3):708–716
54. Smiatek J, Liu D, Heuer A (2012) High temperature unfolding simulations of a single-stranded DNA i-motif. Curr Phys Chem 2(1):115–123
55. Qamhieh K, Wong KY, Lynch GC, Pettitt BM (2009) The melting mechanism of DNA tethered to a surface. Int J Numer Anal Model 6(3):474–488
56. Priyakumar UD, Harika G, Suresh G (2010) Molecular simulations on the thermal stabilization of DNA by hyperthermophilic chromatin protein Sac7d, and associated conformational transitions. J Phys Chem B 114(49):16548–16557
57. Hoover WG (1985) Canonical dynamics—equilibrium phase-space distributions. Phys Rev A 31(3):1695–1697
58. Feller SE, Zhang YH, Pastor RW, Brooks BR (1995) Constant-pressure molecular-dynamics simulation—the Langevin piston method. J Chem Phys 103(11):4613–4621
59. Halder S, Bhattacharyya D (2010) Structural stability of tandemly occurring noncanonical basepairs within double helical fragments: molecular dynamics studies of functional RNA. J Phys Chem B 114(44):14028–14040
60. Bansal M, Bhattacharyya D, Ravi B (1995) NUPARM and NUCGEN—software for analysis and generation of sequence-dependent nucleic-acid structures. Comput Appl Biosci 11(3):281–287
61. Mukherjee S, Bansal M, Bhattacharyya D (2006) Conformational specificity of non-canonical base pairs and higher order structures in nucleic acids: crystal structure database analysis. J Comput Aided Mol Des 20(10–11):629–645
62. Olson WK, Bansal M, Burley SK, Dickerson RE, Gerstein M, Harvey SC, Heinemann U, Lu XJ, Neidle S, Shakked Z, Sklenar H, Suzuki M, Tung CS, Westhof E, Wolberger C, Berman HM (2001) A standard reference frame for the description of nucleic acid base-pair geometry. J Mol Biol 313(1):229–237
63. Dickerson RE, Bansal M, Calladine CR, Diekman S, Hunter WN, Kennard O, von Kidzing E, Lavery R, Nelson HCM, Olson WK, Saenger W, Shakked Z, Skenar H, Soumpasis DM, Tung CS, Wang AHJ, Zurkin VB (1989) Definitions and nomenclature of nucleic acid structure parameters. EMBO J 8(1):1–4
64. Halder S, Bhattacharyya D (2013) RNA structure and dynamics: a base pairing perspective. Prog Biophys Mol Biol 113(2):264–283
65. Wang JC (1979) Helical repeat of DNA in solution. Proc Natl Acad Sci USA 76(1):200–203
66. Bhattacharyya D, Bansal M (1989) A self-consistent formulation for analysis and generation of non-uniform DNA structures. J Biomol Struct Dyn 6(4):635–653
67. Kanhere A, Bansal M (2003) An assessment of three dinucleotide parameters to predict DNA curvature by quantitative comparison with experimental data. Nucleic Acids Res 31(10):2647–2658
68. Skjaerven L, Martinez A, Reuter N (2011) Principal component and normal mode analysis of proteins; a quantitative comparison using the GroEL subunit. Proteins 79(1):232–243
69. Sprous D, Zacharias W, Wood ZA, Harvey SC (1995) Dehydrating agents sharply reduce curvature in DNAs containing A tracts. Nucleic Acids Res 23(10):1816–1821
70. Fritsch V, Westhof E (1991) 3-Center hydrogen-bonds in DNA—molecular-dynamics of poly(dA).poly(dT). J Am Chem Soc 113(22):8271–8277
71. McConnell KJ, Beveridge DL (2001) Molecular dynamics simulations of B′-DNA: sequence effects on A-tract-induced bending and flexibility. J Mol Biol 314(1):23–40
72. Strahs D, Schlick T (2000) A-tract bending: insights into experimental structures by computational models. J Mol Biol 301(3):643–663
73. Hud NV, Polak M (2001) DNA-cation interactions: the major and minor grooves are flexible ionophores. Curr Opin Struct Biol 11(3):293–301
74. Ghosh A, Bansal M (1999) C–H···O hydrogen bonds in minor groove of A-tracts in DNA double helices. J Mol Biol 294(5):1149–1158
75. Kundu S, Roy D (2010) Structural study of carboxylesterase from hyperthermophilic bacteria *Geobacillus stearothermophilus* by molecular dynamics simulation. J Mol Graph Model 28(8):820–827
76. Sponer J, Burcl R, Hobza P (1994) Interactions between amino-groups in DNA—an ab initio study and a comparison with empirical potentials. J Biomol Struct Dyn 11(6):1357–1376
77. Bandyopadhyay D, Bhattacharyya D (2006) Estimation of strength in different extra Watson–Crick hydrogen bonds in DNA double helices through quantum chemical studies. Biopolymers 83(3):313–325
78. Mitra P, Chakraborty B, Bhattacharyya D, Basu S (2013) Excimer of 9-aminoacridine hydrochloride hydrate in confined medium: an integrated experimental and theoretical study. J Phys Chem A 117(7):1428–1438
79. Long H, Kudlay A, Schatz GC (2006) Molecular dynamics studies of ion distributions for DNA duplexes and DNA clusters: salt effects and connection to DNA melting. J Phys Chem B 110(6):2918–2926